Serican Journal of Medicine
2026, VOL. 3, NO. 2, 25240
https://doi.org/10.17161/sjm.v3i2.25240

Expression of PGK1 in Breast Cancers Alters Their Sensitivity to Ferroptosis Induction via Metabolic Reprogramming

Felix Oyelami[1], Andrew Shinkle[1], Chrispus Ngule[1], Folake Oyelami[2], Oluwafunminiyi Obaleye[1], Amos Akinyemi[1], Tijesunimi Oyetunde, Samuel Nwadialo[1], Xiongjian Rao[1], Xingcong Ren[1] and Jin-Ming Yang[1#]

[1]Department of Toxicology and Cancer Biology, Department of Pharmacology and Nutritional Science, and Markey Cancer Center, University of Kentucky College of Medicine, Lexington, KY 40536, USA; [2]Department of Microbiology, Faculty of Life Sciences, University of Ilorin, Ilorin, Kwara State, Nigeria, 1515.
[#] **Correspondence to:** Jin-Ming Yang, PhD, 1095 V.A. Drive, 306 Health Science Research Building, Lexington, KY 40536-0305. Tel: +1 859 562 2154; Fax: +1 859 257 6030; E-mail: jyang@uky.edu

ABSTRACT

Therapeutic resistance and recurrence are primary contributors to poor outcomes in breast cancer patients. Induction of ferroptosis, a type of cell death characterized by an overload of toxic lipid peroxides, has been appreciated as a viable strategy in the treatment of breast cancers, including lethal subtypes such as triple-negative breast cancer (TNBC). Notwithstanding, some cancer subtypes are resistant to ferroptosis, and the underlying mechanisms remain incompletely understood. The current study shows that phosphoglycerate kinase 1 (PGK1), a glycolysis-regulating enzyme, is highly expressed in advanced tumor stages and correlates with ferroptosis resistance as well as poor outcomes, especially in TNBCs. Using genetic and pharmacological approaches, we demonstrated that PGK1 depletion attenuates ferroptosis resistance in TNBC and luminal breast cancer cell lines. We also showed that PGK1 depletion destabilizes GPX4, an anti-ferroptosis defense peroxidase in parallel with pyruvate dehydrogenase (PDH), to disrupt redox homeostasis and enhance lipid peroxidation. In orthotopic TNBC models, we showed that tumoral loss of PGK1 enhances activity of the ferroptosis inducer imidazole ketone erastin (IKE) and reduces tumor size and metastasis. These results indicate that PGK1 plays a key role in modulating breast cancer sensitivity to ferroptosis induction, suggesting that this kinase may be exploited as a therapeutic target to overcome resistance to ferroptosis inducers in breast cancers.

ARTICLE HISTORY
Received: March 13, 2026
Revised: April 12, 2026
Accepted: April 13, 2026

KEYWORDS
PGK1, ferroptosis, GPX4, breast cancer

1. Introduction

Therapy resistance and tumor recurrence are the main causes of mortality in breast cancer patients [1, 2]. Increasing evidence has shown that metabolic reprogramming enables cancer cells to survive in hostile microenvironments, sustain growth and proliferation, and eventually escape death [3-5]. Consequently, targeting vital metabolic regulators to enhance cancer cell death has been regarded with great potential for the treatment of aggressive cancers, including lethal subtypes such as triple-negative breast cancer (TNBC) [6-8]. Ferroptosis is a non-apoptotic and iron-driven type of programmed cell death distinguished by an overload of toxic lipid peroxidation and disruption of redox. Inducing ferroptotic-cell death for the treatment of various cancers has been extensively explored in recent times. In this study, we show that phosphoglycerate kinase 1 (PGK1), a key glycolytic enzyme and regulator [9-11], is overexpressed in breast cancers, including TNBC, and promotes their resistance to ferroptosis induction. In both *in vitro* and *in vivo* experiments, we demonstrate that PGK1 depletion by RNA interference or its inhibition by a small-molecule inhibitor sensitized tumor cells to ferroptosis induction, and that this sensitization is mediated through metabolic reprogramming. PGK1 depletion attenuated pyruvate dehydrogenase (PDH) expression, which elevates metabolic stress, extracellular acidification, and lipid peroxidation, enhancing ferroptosis. Ferroptosis-resistant tumor cells exhibited higher PDH expression, maintained their oxidative metabolism and redox

homeostasis, and showed a decreased susceptibility to ferroptosis induction. These observations imply that targeting PGK1 in combination with ferroptosis induction may be exploited as a novel strategy for the treatment of ferroptosis-insensitive breast cancer and likely other types of tumors.

2. Materials and Methods

Reagents

Erastin (MedChemExpress, NJ, USA, #HY-15763), Imidazole ketone erastin (MedChemExpress, NJ, USA, #HY-114481), NG52 (MedChemExpress, NJ, USA, #HY-15154,), Ferrostatin (MedChemExpress, NJ, USA, #HY-100579), Laemli lysis buffer, RIPA lysis buffer, Complete protease inhibitor (Roche, MH, GERMANY, # 0469331001), Dimethyl Sulfoxide (DMSO) (VWR, PA, USA, #0231), Triton X-100 (SIGMA ALDRICH MO, USA, #T8787, RRID: AB_2629483) Aquabluer solution (BocaScientific, Wahington, MA, USA, #6015, RRID: AB_12345678), Necrostatin (Selleck, TX, USA, #S8037), Liproxstatin (Selleck, TX, USA, #S7699), Bovine serum albumin (Santa Cruz Biotechnology, TX, USA, #sc-2323A), N-Acetyl cysteine (SIGMA ALDRICH MO, USA, #A9164), Z-VAD FMK (Selleck, TX, USA, #S7023), C11-BODIPY 581/591 (Thermo Fisher Scientific, Waltham, MA, USA, #D3861), 4-Hydroxynonenal (R&D Systems, Minneapolis, MN, USA, #MAB3249, RRID: AB_177699), mirVana™ MiRNA isolation kit (Thermofisher Scientific, VL, Lithuania, # AM1561). DAPI (Thermofisher Scientific, VL, Lithuania, # P36941, RRID: AB_2629482) jetPRIME Transfection Reagent (Polyplus-satorius, IL, FRANCE), PGK1 siRNA (Dharmacon, CA, United Kingdom, #5230), PGK1 siRNA (Santa Cruz Biotechnology, TX, USA, #sc-36215), Crystal violet (SIGMA ALDRICH MO, USA, #C3886, RRID: SCR_015456), MojoSort™ Mouse CD8 T cell Isolation Kit (Biolegend, CA, USA, #480008) PGK1 shRNA (m) Lentiviral Particles (Santa Cruz Biotechnology, TX, USA, # sc-36216-V), Glutathione Peroxidase 4 expression plasmid (OriGene Technologies, Rockville, MD, USA, #RC208065), NADP/NADPH-Glo™ Assay kit (Promega, Madison, WI, USA, #G9081). Z57346765 (MedChemExpress, NJ, USA, HY-W195984). Bicinchoninic Acid (BCA) assay kit (Thermos Scientific, Waltham, MA, USA, #23228), AdvanBlock™-Chemi Blocking Solution (Advansta, CA, USA, #R-03726-E10).

Antibodies

PGK1 (Santa Cruz Biotechnology, TX, USA, #sc-130335, RRID: AB_2165228), PGK1 (NOVUS biological, CO, USA, #NBP2-19784, RRID: AB_2786860), ACSL4 (Santa Cruz Biotechnology, TX, USA, #sc-365230, RRID: AB_10847863), GPX4 (Santa Cruz Biotechnology, TX, USA, #sc-166437, RRID: AB_2279252), FSP1 (AMID) (Santa Cruz Biotechnology, TX, USA, #sc-376594, RRID: AB_11149443), BMAL1 (Santa Cruz Biotechnology, TX, USA, #sc-365645, RRID:AB_RRID:AB_10842165), Pyruvate Dehydrogenase (Cell Signaling Technology, MA, USA, #2784, RRID: AB_2061989), PKM1/2 (Cell Signaling Technology, MA, USA, #3186, RRID:AB 2162606), PKM2 (Cell Signaling Technology, MA, USA, #3186, RRID:AB 1904096),b-Actin (Cell Signaling Technology, MA, USA, #3700, RRID: AB_2242334), LDHA (Cell Signaling Technology, MA, USA, #3582, RRID:AB_10694487), Ferritin (Santa Cruz Biotechnology, TX, USA, #sc-376594, RRID:AB_11149443).

Bioinformatics Analysis

To investigate the expression patterns and clinical significance of PGK1 in breast cancer cell lines, publicly available datasets such as RNA-seq data from the TCGA, together with GEO datasets, were obtained using cBioPortal (RRID: SCR_014555) for transcriptomic profiling and copy number variation analysis. Expression patterns of PGK1 in the luminal, HER2-positive, basal, and triple-negative breast cancer (TNBC) subtypes were evaluated relatively to normal breast tissues. Clinical outcome data, such as Overall Survival (OS), Post-Progression survival (PPS), and Relapse-Free Survival (RFS), were acquired from a total of 4,929 breast cancer patients' data at the TCGA Pan-Cancer Clinical Data Resource (TCGA-CDR) using the KM Plotter tool (https://kmplot.com/analysis/index.php?p=service) [12]. To obtain the PGK1 protein expression levels, UALCAN (RRID: SCR_018826) was used to analyze Clinical Proteomic Tumor Analysis Consortium (CPTAC) data, particularly in stage-specific and subtype-specific breast tumors relative to normal tissues. Breast cancer patients were ranked into high and low PGK1 expression groups, then the prognostic relevance of PGK1 was examined using the Kaplan-Meier Plotter (RRID: SCR_018753), which evaluated the overall survival (OS) and Relapse-free survival (RFS) between the groups. Furthermore, ferroptosis-linked

gene signatures from GEO datasets were investigated to explore the association between PGK1 expression and ferroptosis resistance.

Cell culture

MCF7 (RRID: CVCL_0031), MDAMB231 (RRID: CVCL_0062), BT549 (RRID: CVCL_1092), MDAMB468 (RRID: CVCL_0419), and cells were acquired from ATCC (ATCC, VA, USA). HCC70 (RRID: CVCL_1258), T47D (RRID: CVCL_0553), HCC1187 (RRID: CVCL_1248), and MDAMB453 (RRID: CVCL_0418) were kind gifts from Dr Wu Yadi. L2T lentiviral particles were kind gifts from Dr Xia Liu. For in vitro experiments, Cells were cultured in RPMI, DMEM-F 12, or High-glucose DMEM (Invitrogen, Carlsbad, CA, USA) supplemented with 10% fetal bovine serum (FBS, Sigma-Aldrich, St. Louis, MO, USA) and incubated at 36.7 ˚C with 5% CO2. For drug treatment, 5,000 cells were treated with various concentrations of erastin (0, 0.5, 1, 2, 4, 10, 20, 40, 80 μM) for up to 72 hours. To interfere with ferroptosis and other cell death mechanisms, cells were treated with erastin alone or in combination with NG52 (5μM) or Z57346765 (25 μM) cell death inhibitors, such as ferrostatin (20μM), Liproxstatin (1 μM), Necrostatin (20 μM), Zvad-FMK (100 μM), and NAC (20 mM) as described previously [13].

Western blotting

Cells were collected into cold phosphate-buffered saline, spun down, and protein was extracted in Laemmli or RIPA buffer supplemented with protease inhibitor. Protein concentration was evaluated using a BCA assay kit. Cell lysates were run in sodium dodecyl sulphate-polyacrylamide gel electrophoresis (SDS-PAGE) at 100 volts for 2-2:30 hours. Proteins were transferred onto an Immobilon PVDF or nitrocellulose membrane in a transfer buffer at 100 volts for 1:10 hours. Membranes were blocked in 5% defatted milk in PBST or Chemi blocking solution for one hour, and blots were incubated overnight with appropriate primary antibody at 4 ˚C with gentle rocking. Horse-radish Peroxidase (HRP)- secondary antibody was incubated at room temperature for 1 hour, followed by two washes in PBST for 15 minutes each. Protein expression levels were visualized using the ChemiDOC™ MP imaging system (BioRad, Hercules, CA, USA)

Quantitative Real-time PCR

RNA was extracted from the cell pellets using an Invitrogen mirVana™ MiRNA isolation kit (Thermofisher Scientific, Vilnius, Lithuania, # AM1561). First-strand cDNA was produced from 2μg of total RNA using Invitrogen SuperScript™ IV First-strand Synthesis System (Thermofisher Scientific, Vilnius, Lithuania, #18091050), and qRT-PCR was performed using the 7500 Fast Real-Time PCR System (Applied Biosystems, Foster City, CA, USA).

Seahorse Analysis

Extracellular Acidification Rate (ECAR) was investigated using the Seahorse Bioscience Extracellular Flux Analyzer (XF 96 Agilent, RRID: SCR_019545). MCF7, MDAMB231, and MDAMB468 cells were seeded at densities of 5000, 15,000, and 20,000, respectively, in 200μl of DMEM, and allowed to adhere overnight in 96-well Seahorse plates. Cells underwent experimental conditions and were incubated for an additional 48hours. Cells were washed and incubated in a Seahorse assay medium for one hour at 37°C in a CO2-free incubator to equilibrate. The assay was subsequently performed according to the standard Glycolysis stress test protocol with procedural injections of glucose, oligomycin, and 2-deoxyglucose (2-DG). ECAR was evaluated at baseline level and after each injection to assess glycolytic flux. The data acquired were normalized and analyzed using Seahorse Wave software (RRID: SCR_014526).

Immunocytochemistry (ICC) and Immunofluorescence Assays

Tumor cells (2×10^5 cells/ml) were seeded on sterile round coverslips that were placed in a 24-well plate and treated following the experimental procedure. The cells were then fixed with 300 μL of cold methanol (-10 ˚C) for 5 mins, air dried, and permeabilized with 0.25% Triton X-100 in PBS for 10 mins. Next, the cells were blocked with blocking solution (2% Bovine Serum Albumin + 0.1% Triton X-100 in PBS) for 1 hr at room temperature, incubated overnight at 4 ˚C with primary antibodies diluted in blocking solution according to the manufacturer's instructions. Subsequent steps were performed in a protected environment from light. The cells were washed three times with 1X PBS, then incubated with secondary antibodies diluted 1:500 in blocking solution for 1 hr at room temperature. Cells were washed with 1X PBS for 5 mins, incubated in DAPI (300 nM) at room temperature for 5 mins, and washed for another 5 mins with 1X PBS. Slides were mounted on a carrying glass and stored overnight at 4°C in dark

conditions. For tissues, formalin-fixed paraffin-embedded (FFPE) tumor resections from *Balb/c* mice were processed by the biospecimens core facility of the University of Kentucky according to the approved Institutional Review Board (IRB) protocol. Tissue sections were deparaffinized, progressively rehydrated through graded ethanol, and subjected to heat-induced antigen retrieval using sodium citrate buffer (pH 6.0) for 12 minutes. Next, sections were twice blocked in 100mM glycine for 8 minutes each, washed twice in PBS, and blocked in 10% normal donkey serum in 1% BSA for 1 hour at room temperature. Sections were incubated in primary antibodies (1:50) overnight at 4 °C, followed by two washes in PBST, then 1 hour of incubation in appropriate secondary antibodies (1:1000) at room temperature. Following two washes with PBST, nuclei were counterstained with DAPI for 5 minutes, washed once, and then mounted using aqueous mounting medium. Imaging was done under identical exposure settings for all treatment groups.

4-Hydroxynonenal (4-HNE) Immunohistochemistry and Quantification

Formalin-fixed, paraffin-embedded tissue sections were stained for 4-hydroxynonenal (4-HNE) using an anti-4-HNE antibody. Tissue sections were deparaffinized, progressively rehydrated through graded ethanol, and subjected to heat-induced antigen retrieval using sodium citrate buffer (pH 6.0) for 12 minutes. Sections were blocked and incubated in primary antibody overnight at 4 °C, followed by 1 hour of incubation with appropriate fluorescent secondary antibodies at room temperature. Nuclei were counterstained with DAPI, washed, and slides mounted using an aqueous mounting medium. Imaging was done under identical exposure settings for all treatment groups and quantified using Image-Pro Plus v4.5.

Measurement of intracellular NADPH levels

Intracellular NADPH levels were evaluated according to the manufacturer's instructions of the NADP/NADPH-Glo™ Assay kit. Briefly, breast cancer cells were seeded in 6-well plates and allowed to adhere and undergo treatment conditions for 48hours. Cells were then washed once with cold PBS and lysed directly in the wells using 100 µL of Base Solution (NaOH) supplemented with 1% dodecyltrimethylammonium bromide (DTAB) for efficient cell lysis and preservation of pyridine nucleotides. Lysates were transferred to Eppendorf tubes and divided equally for selective measurement of $NADP^+$ or NADPH. To measure NADPH, selected aliquots were heated at 60 °C for 15 min without acid treatment, which selectively degrades $NADP^+$ while sparing NADPH. Next, samples were cooled to room temperature and neutralized using HCL/Trizma solution.

Neutralized samples were transferred to white opaque 96-well plates, and the NADP/NADPH-Glo™ Detection Reagent was added according to the manufacturer's instructions. NADPH levels were calculated based on Luminescence obtained after reading the plate on a GloMax Discover microplate luminometer (Promega), and values obtained were normalized relative to those of control samples. All experiments were performed with at least three independent biological replicates, and data are reported as mean ± SD.

Lipid peroxidation analysis by C11-BODIPY 581/591 staining

Lipid peroxidation was assessed using the C11-BODIPY 581/591 probe, which undergoes a relative fluorescence change from red (reduced) to green (oxidized) during lipid oxidation. Breast cancer cells underwent treatment conditions and were washed twice in PBS, followed by incubation with 5 µM C11-BODIPY 581/591 in serum-free medium at 37 °C for 30 minutes, protected from light. After staining, cells were washed twice with PBS and analyzed by flow cytometry within 2 hours, whereby Oxidized C11-BODIPY was detected in the FITC (green) channel and reduced C11-BODIPY was detected in the PE (red) channel. Lipid peroxidation was taken as the ratio of FITC to PE fluorescence intensity, and treatment groups were normalized to vehicle-treated controls. Experiments comprised at least three independent biological replicates, and data are reported as mean ± SD.

Cell viability assay

Aquabluer redox indicator for cell viability was used to evaluate cell viability. Briefly, 5×10^4 control or PGK1-depleted (siRNA-transfected or NG52-treated) cells were seeded into 100µl of growth medium per well in 96-well plates and then treated with erastin alone or in combination with Fer-1 (20 µM), Lip-1 (1 µM), Nec-1 (20 µM), Z-Vad-FMK (100 µM), n-acetyl cysteine (20 µM), and cultured for 72 hours. Afterwards, cells were cultured in 100µl of reconstituted Aquabluer solution, incubated for four hours,

and the absorbance was measured at 450 nm by a microplate reader to evaluate cell viability. All drugs were dissolved in DMSO and further diluted in cell culture media according to experimental needs. The final concentration of DMSO in all experiments did not exceed 0.5% (v/v), and control groups were treated with proportionate amounts to serve as a baseline for normalization.

Colony formation assay

200 control or PGK-depleted MCF7, MDAMB468, and 4T1 cells were seeded in a 12-well flat-bottom plate and allowed to adhere overnight. Then, the cells were treated with DMSO as controls or 1.25μM of erastin for 14 days. Afterwards, the cells were fixed in 4% PFA for 14 minutes, stained with crystal violet solution for 15 minutes, rinsed with double-distilled water, and air-dried at room temperature for later visualization of the colonies.

Cell transfection

MCF7 and MDAMB231 cells were transfected with 800nm of PGK1 siRNA using jetPRIME Transfection Reagent. Following transfection, cells were incubated at 37˚C for 72 hours before experimental use. L2T lentiviral particles were transfected into 4T1 cells at a concentration of 40 μg/ml with Polybrene (10 μg/ml) overnight, then the cells were allowed to recover for 3 days and expanded before experimental use. Stable PGK1 knockdown cell lines were generated by transfecting 10 μl of mouse PGK1 lentiviral shRNA particles into wild-type 4T1 cells. Thereafter, stable PGK1 knockdown clones were selected with puromycin (10 μg/ml) and expanded before experimental use.

Transient overexpression of GPX4 was performed using a human GPX4 expression plasmid. An empty vector or GPX4 plasmid was maintained in *E. coli* under kanamycin selection (50 μg/ml) according to the manufacturer's instructions. Thereafter, MDAMB468 cells were transfected with the plasmids using Lipofectamine according to the manufacturer's instructions and incubated for 24 hours before subsequent treatment. Successful GPX4 overexpression was first confirmed by western blot analysis before assessment of cell viability and ferroptosis-related endpoints.

Animal Experiments

Animals used in this investigation were treated humanely according to the recommendations established by the American Veterinary Medical Association. The Institutional Animal Care and Use Committee of the University of Kentucky approved all the test protocols (protocol number IBC-24-4). 20 *BALB/c (*RRID: IMSR_JAX:000651*)* mice were orthotopically injected with 1×10^6 L2T-transfected Wild-type or PGK1 knockdown 4T1 cells in their fifth mammary fat pad, and tumor size was monitored and measured every four days. After the tumor volume reached 80-100 mm^3, mice were randomly divided into two groups, each comprising 5 mice. Mice were then intraperitoneally treated with either vehicle (5% DMSO, 4% PEG, 4% Tween-80 in saline) or Imidazole ketone Erastin (40 mg/kg) once every day for 14 days.

Institutional Review Board Statement

The study was conducted according to the guidelines of the Declaration of Helsinki and approved by the Institutional Review Board of the University of Kentucky (protocol code IBC-24-4 JMY; Date approved: 01.28.2025).

In accordance with our approved Institutional Animal Care and Use Committee (IACUC) protocol, tumor-bearing mice were monitored closely and euthanized when tumor volume reached 1 cm in diameter or earlier if signs of distress were observed.

Statistical analysis

Statistical analysis was performed using GraphPad Prism version 10.4.1 (GraphPad Software, CA, USA). All experimental studies comprised at least three independent experiments represented as mean ± SD. *The t*-test was used for two groups, and Analysis of Variance (ANOVA) for multiple groups. Significance was defined as a p-value <0.05 between the experimental and control groups.

3. Results

3.1 High PGK1 expression in breast cancer is associated with poor prognosis and ferroptosis insensitivity.

We observed that PGK1 was expressed at different levels among subtypes of breast cancer cell lines, even within similar categories of breast cancers (Fig. 1A). Using Xena browser, we analyzed the comprehensive datasets from the Cancer Genome Atlas Program (TCGA). In the TCGA samples, of which the majority are primary tumor tissues, PGK1 expression was higher in breast tumor tissues than in their normal counterparts. In the 1097 samples, we observed

Fig. 1. High PGK1 expression is associated with poor prognosis and ferroptosis resistance in breast cancer patients. A. Western blotting of PGK1 in TNBCs and non-TNBC cell lines. B. Gene expression levels of PGK1 in normal versus breast cancer primary tumors in TCGA datasets. C. Gene expression levels of PGK1 in normal, luminal, HER2, and TNBC tissues in the TCGA dataset samples. D. PGK1 expression across different stages of breast cancer. E. Effect of PGK1 expression on overall survival of patients with breast cancer, as analyzed using Kaplan Meier Plotter. F. Abundance profile for PGK1 across sensitive vs ferroptosis-resistant cancers in a GEO dataset. Data represent mean ± SD; one-way ANOVA, ns: not significant, * $p < 0.05$, ** $p < 0.01$, *** $p < 0.001$, **** $p < 0.0001$. Note: The data shown in panel (1A) were obtained from an independent experimental repeat to avoid redundancy with Figure 2A.

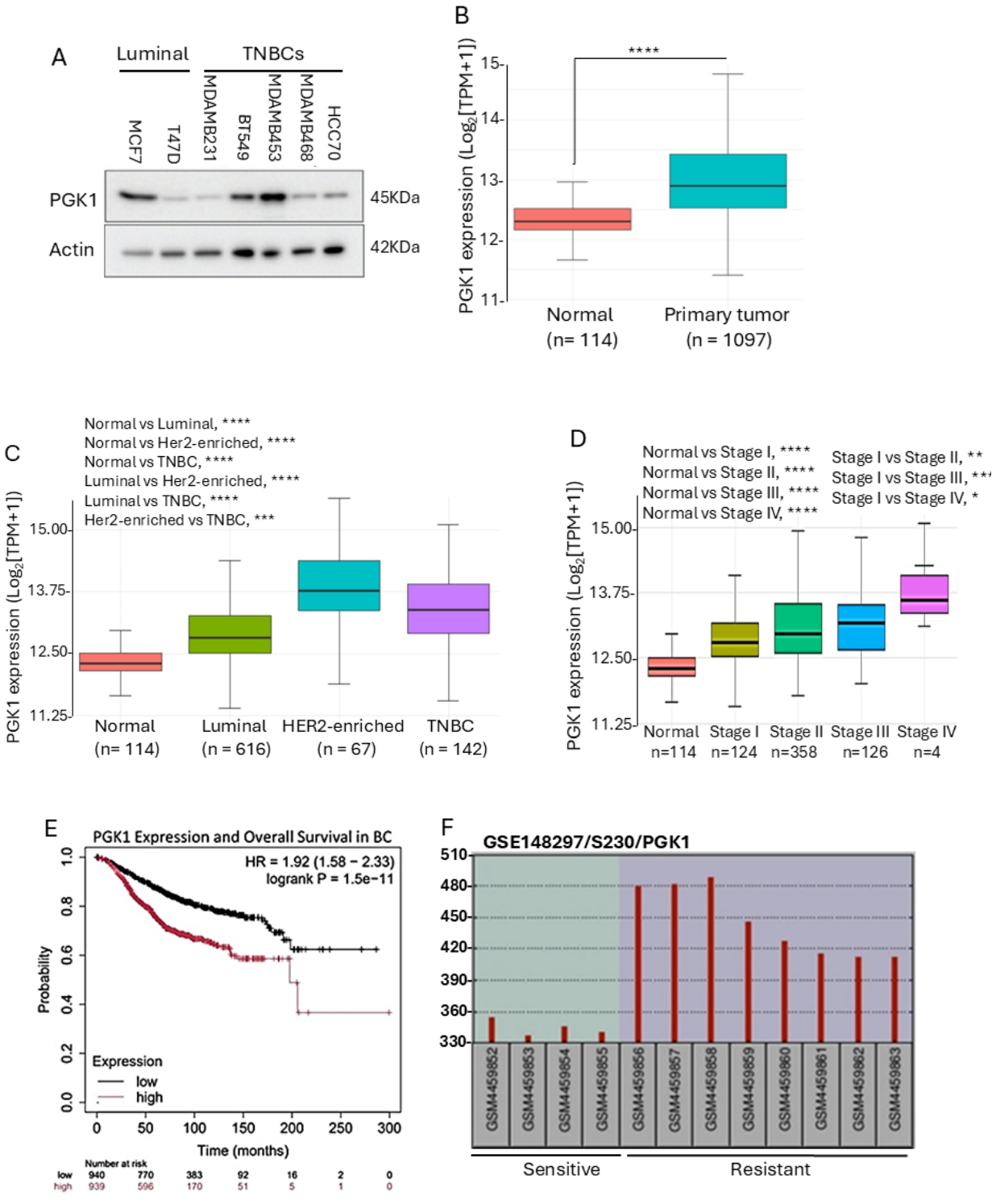

Table 1: Viability measurement of human triple-negative breast cancers MDAMB231, BT549, MDAMB468, MDAMB453, HCC1187, and luminal cancers T47D and MCF7 cell lines treated with increasing doses of erastin for 72 hours. Data is represented as the mean ± SD (n = 6).

Cell line	Category	IC50 (μM ± SEM)
MDAMB231	Triple-Negative	4.8
BT549	Triple-Negative	6.0
MDAMB468	Triple-Negative	9.0
MDAMB453	Triple-Negative	22.0
HCC1187	Triple-Negative	41.0
HCC70	Triple-Negative	>60.0
T47D	Luminal	>60.0
MCF7	Luminal	>60.0

that the expression of the PGK1 gene (transcripts per million) were at least 1.5-fold higher ($p < 0.05$) in the human primary tumors than in the normal breast tissue (Fig. 1B). As breast cancer is highly heterogeneous and its prognosis varies among different subtypes of the disease, we performed bioinformatic analysis of PGK1 expression in different subtypes of breast cancer. We grouped PGK1 expressions of the TCGA *pan*-cancer datasets into luminal, HER2, triple-negative tumors, and normal breast tissues. Fig. 1C shows that PGK1 expression was highly expressed in TNBCs and HER2 samples as compared to other subclasses of breast cancer. Also, we observed a progressive increase in PGK1 expression as tumors advanced, with the highest PGK1 expression detected in stage IV cancers (Fig. 1D). Using the Kaplan Meier plotter, we stratified the breast cancer samples from 4929 patients into two groups based on PGK1 expression level: high expression group and low expression group. The patients with high PGK1-expressing tumors had lower survival than the patients with low PGK1-expressing tumors (Fig. 1E). Notably, in the datasets from the Gene Expression Omnibus database that were categorized as ferroptosis-sensitive or ferroptosis-resistant based on the immunophenotyping of 12 human 786-0 renal cell carcinoma samples, PGK1 expression was significantly upregulated in the ferroptosis-resistant tumors (Fig. 1F). This analysis was included as supportive, cross-cancer evidence to assess the potential association between PGK1 expression and ferroptosis resistance, rather than to draw breast cancer–specific conclusions. Taken together, these analyses indicate that higher PGK1 gene expression is associated with poorer prognosis, advanced-stage breast cancer, and ferroptosis insensitivity, particularly in TNBC and HER2-positive tumors.

3.2 Expression of PGK1 in breast cancers affects their response to the induction of ferroptosis.

As we observed the heterogenous effects of PGK1 expression on several signaling effectors including GPX4, a regulator of ferroptosis, in breast cancer cells (Fig. 2A), we evaluated the effect of PGK1 expression on ferroptosis activity in breast cancer cells by testing the response of both TNBC cell lines (MDAMB231, MDAMB468 and BT549) and luminal cancer cell lines (MCF7 and T47D) to erastin, a small molecule inducer of ferroptosis**.** Table 1 and Fig. 2B show that TNBC lines MDAMB231, MDAMB468, and BT549 were more sensitive to induction of ferroptosis than the luminal cancer cell lines MCF7 and T47D. We next treated those cell lines with a series of concentrations of NG52, a small molecule inhibitor of PGK1, and observed that IC_{50} values of NG52 in the luminal breast cancer cell lines MCF7 and T47D cell lines were 42 μM and 75 μM, higher than that in the TNBC cells (5 μM, 17 μM and 27 μM for MDAMB231, HCC1187 and MDAMB453, respectively) (Fig. 2C; Table 2), suggesting that TNBC cells are more vulnerable to PGK1 inhibition than the luminal breast cancer cells. The varying responses of HCC70 and HCC1187 compared to other TNBC subtypes reflect the heterogeneity amongst TNBCs. A recent study [14] attributed the different responses to differences in glutathione metabolism, GPX4 expression, and oxidative stress adaptation, implying the importance of considering intragroup heterogeneity when designing ferroptosis-based interventions.

To determine the effect of PGK1 on ferroptosis activity, we measured and compared the ferroptosis markers in tumor cells with or without depletion or inhibition of PGK1. We found that, while Acyl-CoA synthetase long-chain family member 4 (ACSL4), an enzyme involved in regulating fatty acid metabolism

Fig. 2. Depletion of PGK1 Sensitizes Breast Cancer to Ferroptosis. A. Western blotting of ferroptosis biomarkers and PGK1 signaling in TNBCs and non-TNBC cell lines. **B.** Dose-response curve of the ferroptosis inducer erastin in breast cancer cells. **C.** Dose-response curve of the PGK1 inhibitor NG52 in breast cancer cells. **D.** Western Blotting of ferroptosis biomarkers, PGK1 and its downstream targets in control and PGK1-depleted MCF7 and MDAMB231 carcinomas. **E.** Expression of GPX4 mRNA in MCF7 and MDAMB231 cells with or without the depletion of PGK1. **F**. Colony formation assay. MDAMB468 colonies after treatment with vehicle, erastin (1.25 μM), NG52(5 μM), or their combination. **G.** Percentage viability analysis of MDAMB468, MDAMB453, HCC70, T47D, MCF7, and MDAMB231 cell lines after treatment with vehicle, Erastin, NG52, or their combination. Cells were treated for 72 hours, except MDA-MB-231 cells, which were treated for 28 hours. Data represent mean ± SD from n = 3 independent experiments.; t-test (panels E), one-way ANOVA (panels F & G), ns: not significant, * $p < 0.05$, ** $p < 0.01$, *** $p < 0.001$, **** $p < 0.0001$.

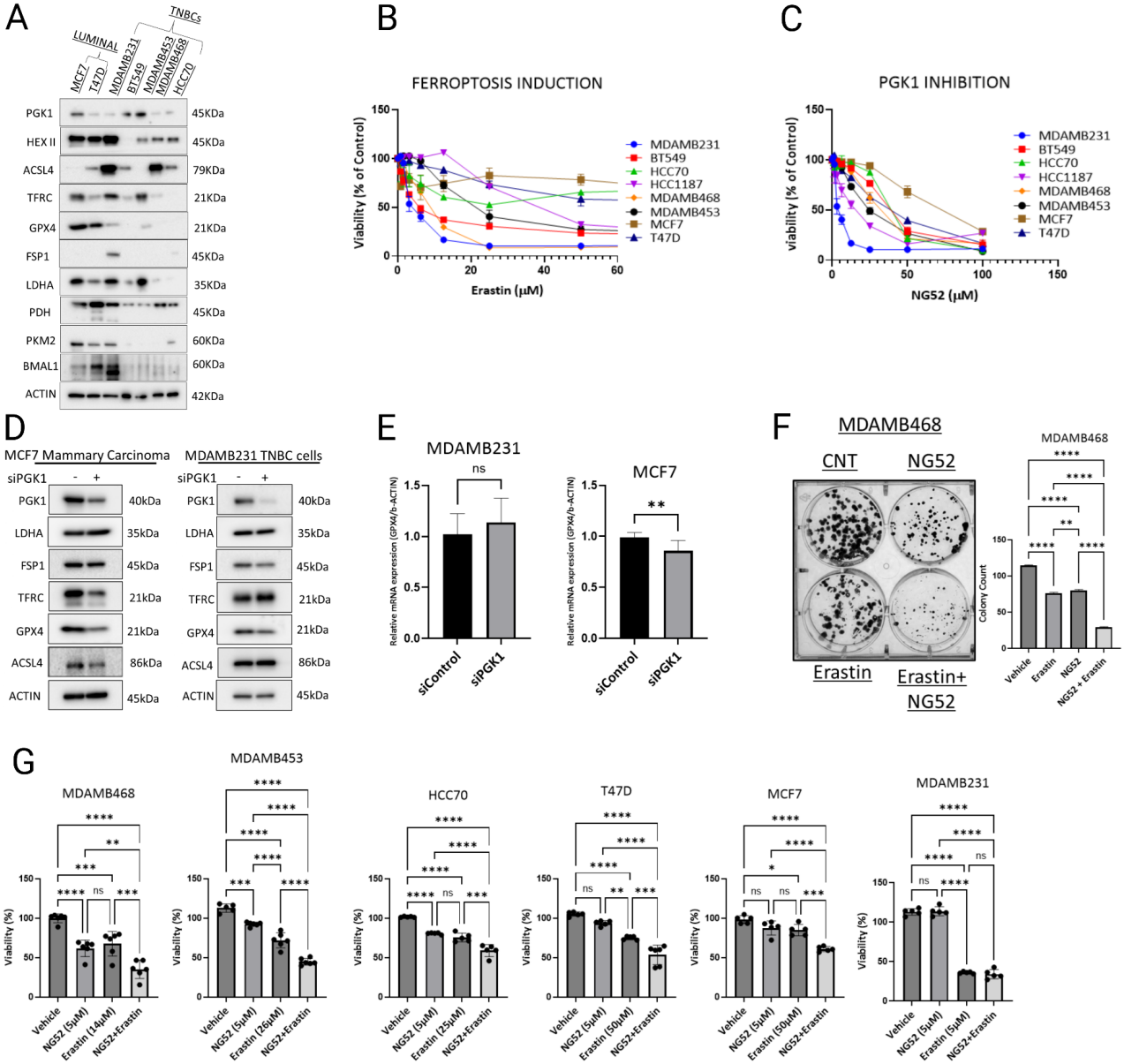

Table 2: Viability measurement of human triple-negative breast cancers MDAMB231, BT549, MDAMB468, MDAMB453, HCC1187, and luminal cancers T47D and MCF7 cell lines treated with increasing doses of PGK1 inhibitor NG52 for 72hours. Data is represented as the mean ± SD (n = 6)

Cell line	Category	IC50 (μM ± SEM)
MDAMB231	Triple-Negative	5.0
BT549	Triple-Negative	40.0
MDAMB468	Triple-Negative	35.0
MDAMB453	Triple-Negative	27.0
HCC1187	Triple-Negative	17.0
HCC70	Triple-Negative	40.0
T47D	Luminal	42.0
MCF7	Luminal	75.0

and a driver of ferroptosis, was downregulated in the PGK1-depleted MCF7 cells but unchanged in the PGK1-depleted MDAMB231 cells. GPX4, an anti-ferroptosis peroxidase, was downregulated in both PGK1-depleted MCF7 and MDAMB231cells (Fig. 2D), suggesting that loss of PGK1 induces a pro-ferroptotic shift through the GPX4 pathway in both cell lines. We also show that PGK1 depletion caused a relocalization of GPX4 to the nucleus (Supp Fig. S1A). PGK1 does not seem to affect the transcription of GPX4 in TNBCs, as GPX4 mRNA levels were comparable between the control and the PGK1-depleted MDAMB231 cells (Fig. 2E). Consistently, depletion of PGK1 sensitized both triple-negative and luminal human breast cancers to the erastin-induced cell death (Supp Fig. 1B & 1C). Notably, ~40% more ferroptotic cell death was observed in MDAMB468 (Fig. 2F) and MDAMB453 cells treated with the PGK1 inhibitor NG52 as compared with erastin alone, but only 20% more ferroptotic cell death was detected in the luminal MCF7 and T47D cells subjected to NG52 treatment (Fig. 2G). To further demonstrate the role of PGK1 in modulating ferroptosis, we generated the MDAMB231 (human TNBC) and 4T1 (murine TNBC) cells subjected to stable knockdown of PGK1 (Supp Fig. 1D) and treated them with the ferroptosis inducer, erastin, in the presence or absence of ferroptosis inhibitors (ferrostatin-1, liproxstatin) or apoptosis inhibitor (ZVAD-FMK). These experiments showed that only the ferroptosis inhibitors, but not the apoptosis inhibitor, prevented cell death, suggesting ferroptosis as the primary cell death mechanism in the PGK1-depleted cells (Supp Fig. 1E & 1F). In addition, treatment with the antioxidant N-acetyl cysteine (NAC), a reactive oxygen species (ROS) scavenger, attenuated cell death under these conditions, further supporting the role of oxidative stress in mediating ferroptosis. Potential off-target effects of NG52 were explored by treating cells with an alternate PGK1 inhibitor, Z57346765. We showed that treatment with Z57346765 showed similar effects of NG52 on viability, metabolic, and ferroptosis-associated markers, supporting the PGK1-dependent mechanism rather than off-target effect (Supp Fig. S3A). These results demonstrate that PGK1 may modulate ferroptosis in breast cancer cells through altering GPX4 level, with TNBC cells showing greater sensitivity to PGK1 depletion.

3.3 PGK1-regulated ferroptosis is associated with metabolism in breast cancer cells.

Since PGK1 is a key glycolytic regulator, we queried whether PGK1 modulates ferroptosis via altering glucose metabolism. We found that with increasing glucose concentrations, ferroptotic activity increased moderately (Fig. 3A). Treatment of both luminal and TNBC cell lines with 2DG, a glycolytic inhibitor, enhanced their sensitivity to the effect of the ferroptosis inducer erastin (Fig. 3B). To determine whether modulation of ferroptosis by PGK1 results from its effect on metabolic signaling, we compared its downstream targets in the control and PGK1-depleted cells under ferroptosis-inducing conditions. We found a consistent downregulation of pyruvate dehydrogenase (PDH) in PGK1-depleted MDA-MB-468 and MCF7 cells, both of which exhibited increased sensitivity to induction of ferroptosis (Fig. 3D & 3E). In contrast, MDAMB231 cells, which did not show increased sensitivity to ferroptosis following PGK1 depletion, displayed an upregulation of PDH expression under the same conditions (Fig. 3C & 2G). Notably, other glycolytic enzymes such as PKM1/2 and LDHA did not show consistent changes across cell lines, which suggests that the PGK1-mediated regulation of ferroptosis was more closely associated with PDH-dependent

Fig. 3. Metabolic changes associated with PGK1-modulated ferroptosis. **A.** Effect of glucose deprivation on viability in breast cancer cell lines during ferroptosis induction. **B.** Effect of glycolysis inhibition on viability in breast cancer cell lines during ferroptosis induction. Western blotting image of ferroptosis biomarkers, PGK1 expression, and its downstream targets after treatment with DMSO, NG52, erastin, or their combination in **C.** MDAMB231, **D.** MCF7, and **E.** MDAMB468. Sea horse assay- ECAR analysis in **F.** MDAMB468 and **G.** MDAMB231 cell lines after treatment with vehicle, erastin, NG52, or their combination. Data represent mean ± SD from n = 3 independent experiments.; one-way ANOVA (panels F, G), ns: not significant, * $p < 0.05$, ** $p < 0.01$, *** $p < 0.001$, **** $p < 0.0001$.

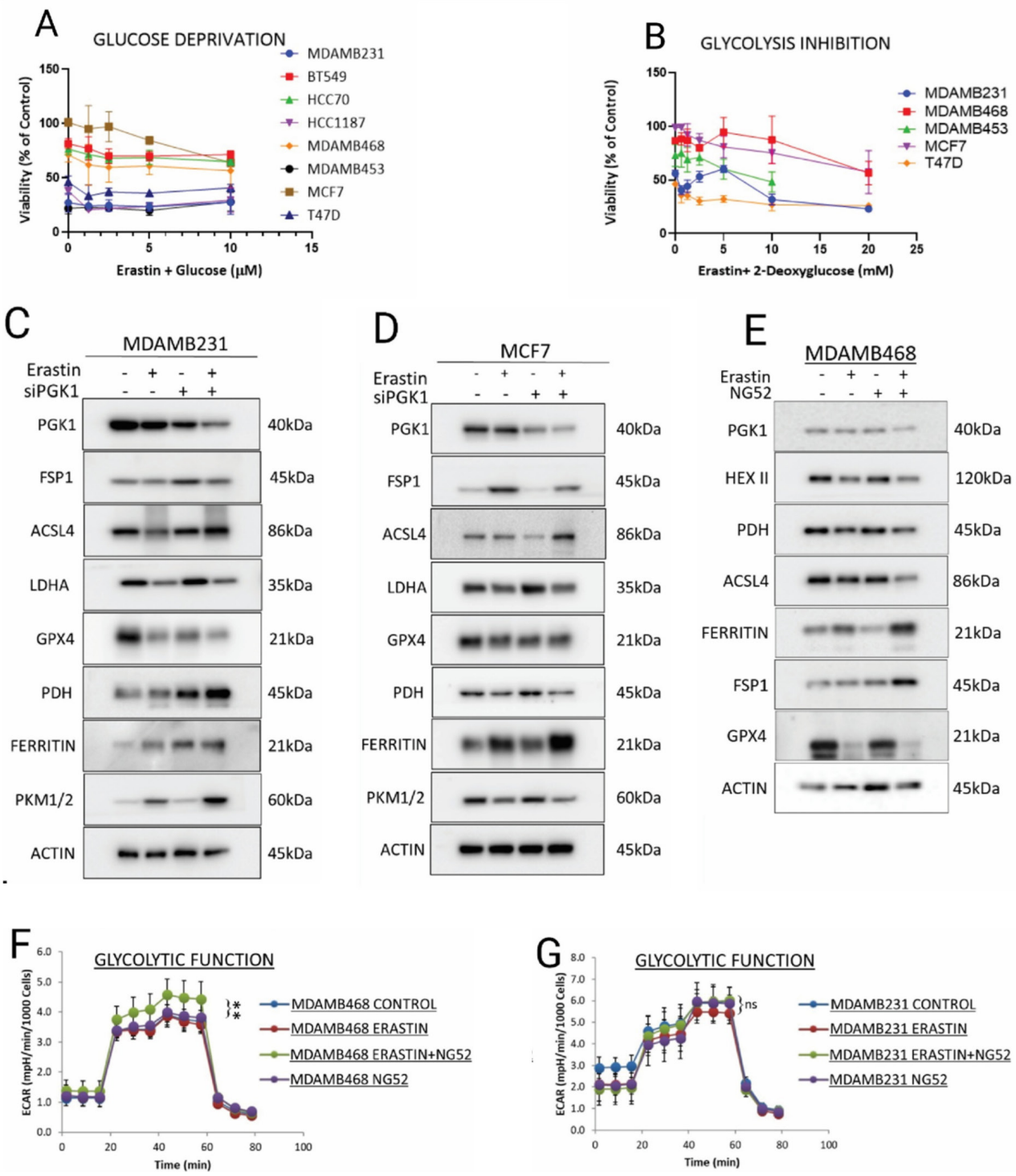

metabolic control rather than global modulation of glycolytic enzymes. This discrepancy might account for the difference in sensitivity to ferroptosis induction among those tumor cells. In addition, we observed an increased ECAR in the PGK1-depleted MDAMB468 cells (Fig. 3F), likely a consequence of a compensatory shift toward glycolysis due to PDH downregulation, limiting pyruvate oxidation. This inefficient adaptation might trigger metabolic stress that enhances ferroptosis sensitivity. On the contrary, the PGK1-depleted MDAMB231 cells, which are ferroptosis-insensitive, upregulated PDH to maintain oxidative metabolism and prevent further sensitization (Fig. 3G).

To further analyze the role of PDH in PGK1-regulated ferroptosis, we treated the PGK1-depleted MDAMB231 cells with hypoxia or oligomycin, an inhibitor of Adenosine triphosphate (ATP) synthase and PDH activity. We show that PDH was substantially down-regulated (Fig. 4A) and the sensitivity to ferroptosis was significantly enhanced in those treated cells as compared with the control cells (Fig. 4B). Similarly, inhibiting PDH in the PGK1-depleted MCF7, MDAMB453, and HCC70 cells sensitized them to the erastin-induced cell death (Fig. 4C). Notably, 30-hour PDH inhibition produced a cell death level nearly comparable to 72-hour ferroptosis induction in the PGK1-depleted cells (Fig. 4C), suggesting PDH upregulation as a possible resistance mechanism. These results imply that PGK1 depletion can sensitize certain subtypes of breast cancer to ferroptosis induction by disrupting metabolic balance, and this sensitization correlates with PDH downregulation. To directly link PGK1 depletion to redox regulation under ferroptotic stress, we measured intracellular NADPH levels using the NADP/NADPH-Glo assay. Fig. 4D shows that PGK1 inhibition significantly reduced NADPH levels in MDAMB468 cells subjected to erastin treatment, an outcome that was partly rescued by ferroptosis inhibitors, suggesting impaired redox buffering capacity during ferroptosis.

In view of the essential role of GPX4 in lipid peroxide detoxification, we determined whether modulation of GPX4 could influence PGK1-dependent ferroptosis in tumor cells. Overexpression of GPX4 in MDAMB468 cell lines restored GPX4 protein levels (Fig. 4E) and significantly reduced erastin and NG52-induced cell death (Fig. 4F), demonstrating a functional rescue of ferroptosis sensitivity. Importantly, GPX4 overexpression did not restore PDH expression under these conditions (Fig. 4G), suggesting that GPX4 and PDH operate as parallel downstream effectors of PGK1-mediated metabolic regulation rather than downstream of each other. Consistent with these observations, PGK1 depletion increased lipid peroxidation across multiple breast cancer cell lines, as evidenced by C11-BODIPY 581/591 oxidation, while this effect was inhibited by ferrostatin-1 or liproxstatin-1 (Fig. 4H), validating ferroptosis-mediated lipid ROS accumulation and redox disruption. Representative flow cytometry plots illustrating these changes are shown in Supplementary Fig. 4B & 4D. Notably, erastin and NG52 co-treatment elevated lipid peroxidation in MDAMB231 without a proportionate loss of viability due to the elevated PDH-mediated redox buffering, which suggests that ROS accumulation alone is not sufficient to drive ferroptosis cell death.

3.4 Targeting tumoral PGK1 enhances the antitumor activity of the ferroptosis-inducing agent.

To assess the importance of the PGK1-regulated ferroptosis *in vivo*, we inoculated mice with the murine TNBC 4T1 cells with or without depletion of PGK1, followed by treatment with either vehicle or imidazole ketone erastin (IKE), a ferroptosis inducer (Fig. 5A). These experiments demonstrated that IKE significantly slowed tumor growth, with a more pronounced reduction in tumor volume in the mice bearing PGK1-depleted tumors as compared with those with tumors expressing PGK1 (Fig. 5C-5E). Furthermore, IKE treatment completely abrogated lung metastasis in mice bearing the PGK1-depleted 4T1 tumors, whereas mice with control tumors exhibited metastatic progression (Fig. 6A & 6B). Also, immunohistochemical analysis of tumor sections showed a progressive reduction in GPX4 expression across the treatment groups, i.e., GPX4 expression was high in the control 4T1-inoculated (vehicle-treated) tumors, moderately reduced in the control 4T1-inoculated (IKE-treated) tumors, further decreased in the PGK1-depleted 4T1-inoculated (vehicle-treated) tumors, and completely absent in the PGK1-depleted 4T1-inoculated (IKE-treated) tumors (Fig. 6C-6E). Consistent with GPX4 alterations, markedly increased accumulation of the lipid peroxidation marker, 4-hydroxynonenal (4-HNE), was observed in the PGK1-depleted tumors treated with IKE (Supp Fig. S4A).

Fig. 4. Effect of metabolic alteration on the sensitivity of breast cancer cells to induction of ferroptosis. A. Western blotting of ferroptosis biomarkers, PGK1 expression, and its downstream targets in MDAMB231 after treatment with DMSO, NG52, erastin, or their combination under normoxic or hypoxic conditions for 72 hours. **B.** Cell viability analysis of the MDAMB231 cell line after treatment with vehicle, erastin, NG52, or their combination under normoxic and hypoxic conditions for 28 hours. **C.** Cell viability analysis of control and PGK1-depleted HCC70, MDAMB453, and MCF7 cell lines following oligomycin treatment under ferroptosis-inducing conditions for 30 hours. The data shown in this panel (4A) were obtained from an independent repeat of the experiment to ensure result integrity and to avoid redundancy with Figure 3C. **D.** Intracellular NADPH levels in MDAMB468 cells after treatment with DMSO, erastin, NG52, or their combination in the presence or absence of ferroptosis inhibitors. **E.** Western blotting image of PDH and GPX4 expression in MDAMB468 cells transduced with an empty vector or GPX4 overexpression plasmid. **F.** Cell viability analysis of MDAMB468 GPX4-OE cells treated with vehicle, NG52, erastin, or the combination. **G.** Western blotting Image of PGK1, PDH, and GPX4 in MDAMB468 GPX4-OE cells after treatment with DMSO, erastin, NG52, or their combination. **H.** Lipid peroxidation in 4T1, MDAMB231, and MCF7 cells assessed by C11-BODIPY 581/591 staining and expressed as the oxidized/reduced (FITC/PE) fluorescence ratio. Data represent mean ± SD from n = 3 independent experiments.; one-way ANOVA (panels B, C, D, F, H), ns: not significant, * $p < 0.05$, ** $p < 0.01$, *** $p < 0.001$, **** $p < 0.0001$.

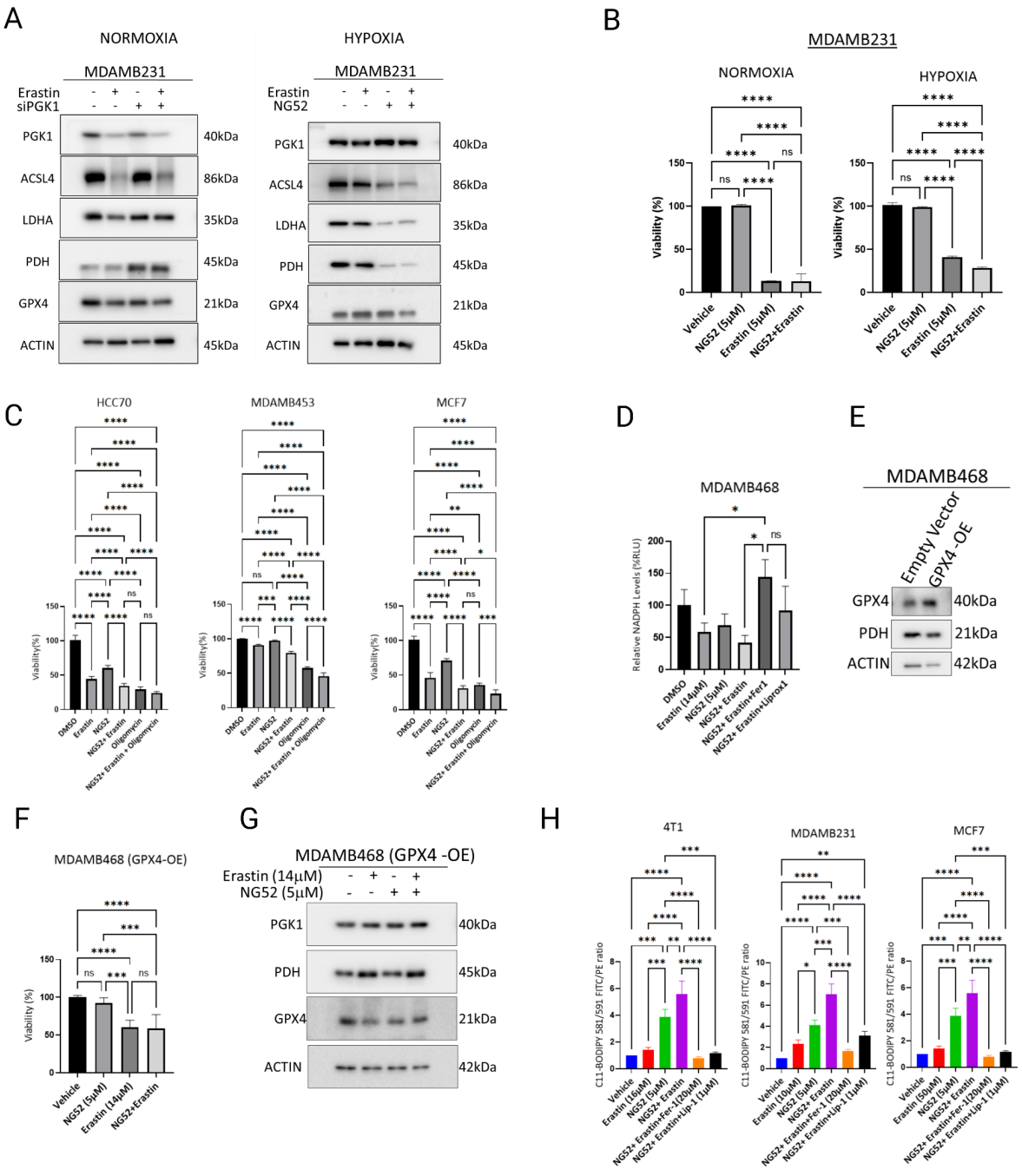

Fig. 5. Targeting of PGK1 enhances ferroptosis in an orthotopic mouse tumor model. A. Orthotopic mouse tumor model. Mice were orthotopically implanted with luciferase-transfected 4T1 murine carcinoma cells (1×10^6 cells/ injection, on the 5th mammary fat pad, n = 5) with or without the depletion of PGK1. On day seven after inoculation, mice were intraperitoneally injected with Imidazole ketone erastin (40 mg/kg) or vehicle once every day for 14 days to induce ferroptosis. Tumor growth was constantly monitored with the Lago imaging system. **B.** Tumor growth rates from Balb/c mice implanted with control or PGK1-depleted L2T-4T1 carcinomas, which were treated with IKE (40 mg/kg) or vehicle. **C.** luminescence intensity of tumor size from mice inoculated with control or PGK1-depleted L2T-4T1 carcinomas and treated with IKE (40mg/kg) or vehicle. **D.** Representative image of tumors collected from mice inoculated with control or PGK1-depleted L2T-4T1 carcinomas and treated with IKE (40 mg/kg) or vehicle, and **E.** their quantitation analysis. Mean ± SD; one-way ANOVA, Tumor growth curves were analyzed by two-way repeated-measures ANOVA followed by Tukey's multiple-comparison test. Data are mean ± SD, n = 5 mice/group (panel B). Mean ± SD from n = 3 independent experiments.; one-way ANOVA (panels E), ns: not significant, * $p < 0.05$, ** $p < 0.01$, *** $p < 0.001$, **** $p < 0.0001$.

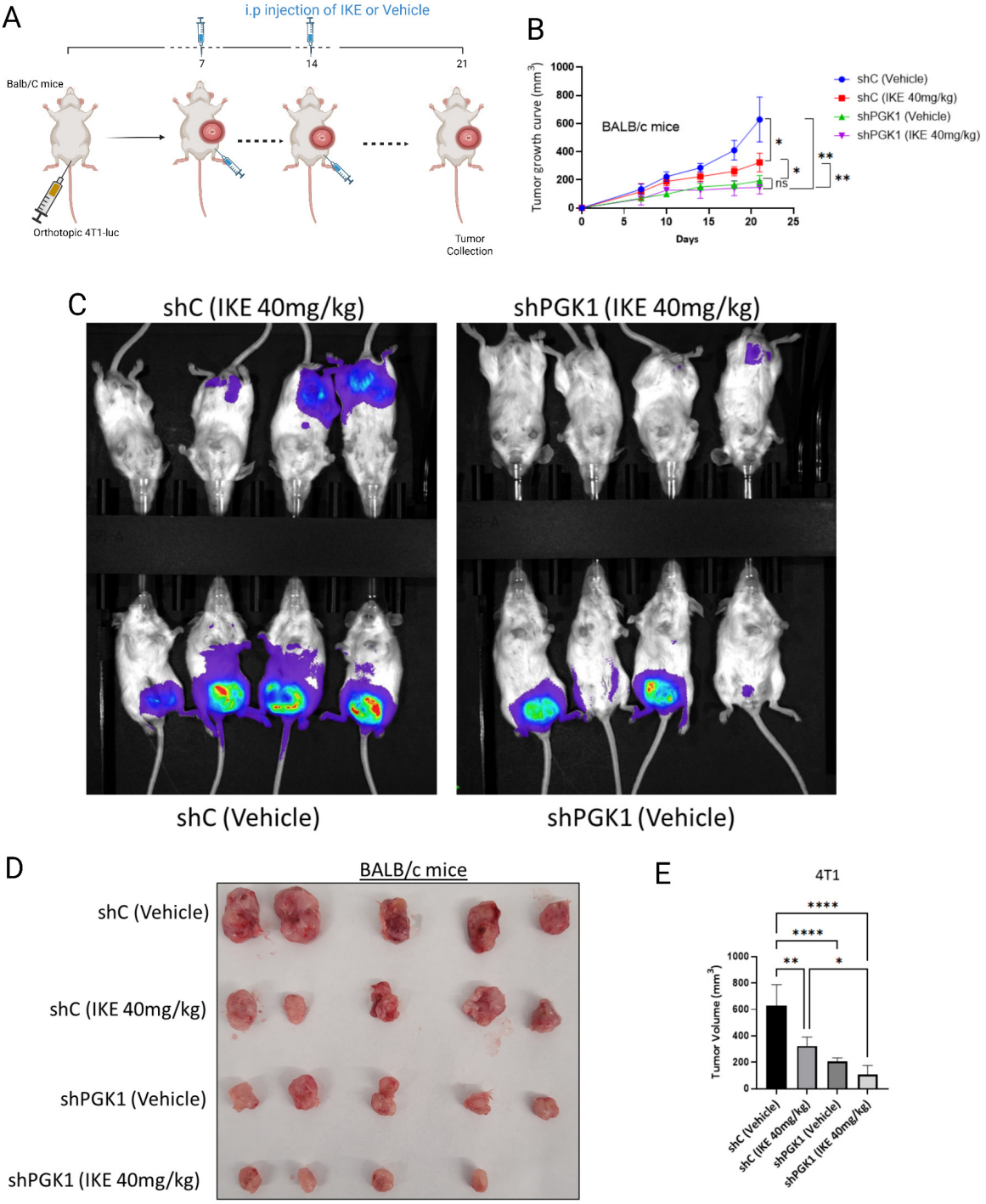

Fig.6. Targeting of PGK1 strengthens antitumor immunity in mouse tumor model. A. Luminescence intensity of L2T-transfected 4T1 carcinoma metastasis in a 24-well organ array plate. **B.** Quantitation analyses of Fig. 6A. **C.** Representative images of tissue section from mice implanted with control or PGK1-depleted L2T-4T1 carcinomas and treated with IKE (40 mg/kg) or vehicle. **D.** Expressions and quantification of GPX4 and **E** Caspase-3 are shown. Data represent mean ± SD from n = 3 independent experiments.; one-way ANOVA (panels B, C, F, H, I), ns: not significant, * $p < 0.05$, ** $p < 0.01$, *** $p < 0.001$, **** $p < 0.0001$.

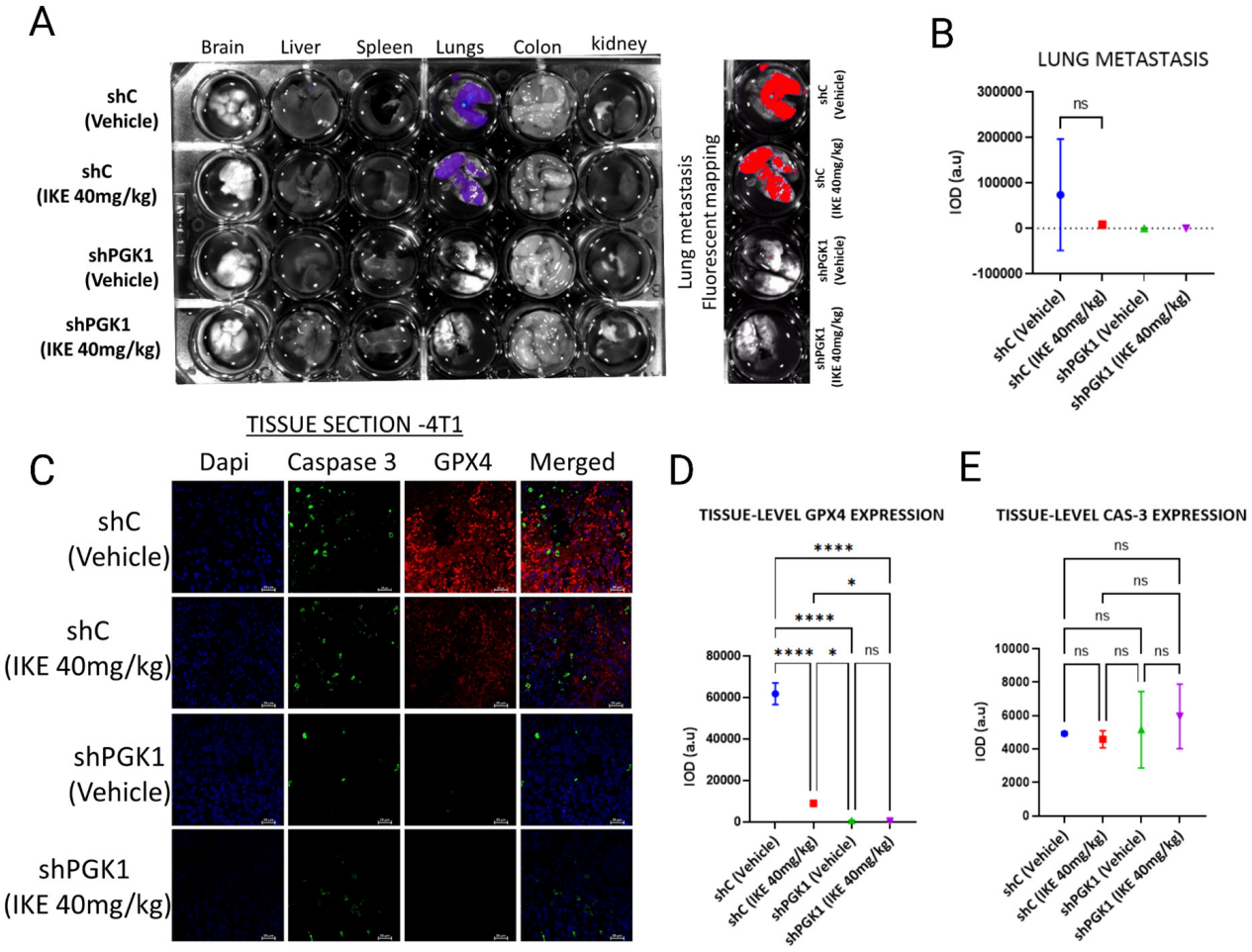

4. Discussion

PGK1 was chosen for this study due to its high expression in aggressive breast cancer subtypes and its links with poor prognosis as seen in the TCGA and GEO datasets. Although prior studies have implicated PGK1 in breast cancer progression [15, 16], its regulation of ferroptosis, an important form of cell death, has not been well elucidated. Our findings show that PGK1 depletion not only destabilizes the ferroptosis regulator GPX4 but also reprograms pyruvate metabolism by modulating PDH levels, which eventually influences the cellular susceptibility to ferroptosis under normoxic and hypoxic conditions. While PGK1 has been reported to exhibit protein kinase activity, whether its kinase function directly mediates the regulation of GPX4 and PDH remains unclear and warrants further investigation. These insights reveal a previously underappreciated role of PGK1 in regulating ferroptosis resistance, offering a novel metabolic target for therapeutic intervention in breast cancer. Our results were obtained primarily from multiple human and murine breast cancer cell models and xenografts. Although the metabolic link between PGK1 activity, redox homeostasis, and ferroptosis may well extend to other cancers, the extent to which this mechanism applies remains to be determined. Even though we used both pharmacologic inhibitors and siRNA-mediated knockdown to prove consistent PGK1-dependent effects, we did not perform rescue experiments using wild-type PGK1. Such an investigation would further strengthen the causal relationship and represent an important direction for future research work. Although TNBCs showed greater vulnerability to ferroptosis compared

to other subtypes, we observed marked differences in sensitivity amongst TNBCs, with opposing responses observed between MDA-MB-231 and MDA-MB-468 cells, likely reflecting innate differences in their metabolic and redox states. These differences perhaps could be attributed to the mesenchymal nature and metabolic plasticity of MDA-MB-231 cell lines, which have a greater reliance on antioxidant defenses such as the glutathione-GPX4 axis, whereas the more basal-like MDA-MB-468 is marked by high EGFR signaling and elevated sensitivity to oxidative stress [17, 18]. Therapy-resistant cancer cells have been widely reported to depend on GPX4-mediated peroxide detoxification [19, 20], a phenomenon that is consistent with the findings of this study. Of note, consistent phenotypes were observed after depleting PGK1 with two distinct inhibitors, which argues against off-target effects and attributes ferroptosis sensitivity to PGK1-dependent metabolic regulation.

The role of PGK1 in cancer remains controversial, with some insights linking its overexpression to oncogenic activities such as tumor progression and therapy resistance [21, 22], and others arguing for its tumoricidal roles, such as its anti-angiogenic disulphide reductase activity in Lewis lung cancer [23]. Notwithstanding, how PGK1 metabolically reprograms tumor cells to survive under ferroptotic conditions remains to be fully elucidated. Accumulating evidence has shown the metabolic underpinnings of ferroptosis, including fatty acid metabolism, iron handling, mevalonate pathway, and thiol metabolism on lipid peroxidation, a catalyst for ferroptosis [24-27]. Here, we show that PGK1 has a role in regulating the levels of ferroptosis markers ACSL4, FSP1, ferritin, and GPX4, the anti-ferroptosis defense peroxidase. Additionally, we show that PGK1 promotes ferroptosis resistance through its downstream target PDH, disagreeing with a previous report that links PDH to ferroptosis-promoting autooxidation of dihydrolipoamides in human fibrosarcoma cells [28]. This discrepancy might be due to cancer-specific roles of PDH under ferroptosis conditions. Nonetheless, we show that PGK1 drives ferroptosis resistance in MDAMB231 by stabilizing PDH under these conditions, which prevents an inefficient compensatory glycolytic shift, metabolic stress, extracellular acidification, and lipid peroxidation, and thereby inhibits ferroptosis. Reduced NADPH availability following PGK1 depletion in the MDAMB468 cell line, for example, provides concrete proof of impaired buffering during ferroptosis.

The different responses observed in MDAMB231 under normoxic conditions compared to hypoxia typify PDH as a vital regulator of ferroptosis susceptibility. Accordingly, PDH expression is sustained under normoxia, which minimizes the combined effect of erastin treatment and PGK1 depletion through the maintenance of redox balance and oxidative metabolism [29-32]. On the other hand, during hypoxia or chemical inhibition of ATP synthase, there is upregulated phosphorylation by pyruvate dehydrogenase kinases (PDKs), which degrades PDH, restricting pyruvate entry into the TCA cycle and causing a metabolic chokepoint that reduces the overall cellular reserve [33]. Indeed, while hypoxia tends to limit the overall ferroptosis extent due to reduced oxygen availability, PDH degradation appears to worsen their metabolically vulnerable state, thereby enhancing the ferroptosis sensitization effect of PGK1 depletion. In parallel, GPX4 governs the ferroptosis threshold by detoxifying lipid peroxides. Hence, when PGK1 depletion impairs glycolytic compensation and PDH loss constrains mitochondrial metabolism, the buffering capacity that supports GPX4 is reduced, thereby sensitizing cells to lipid peroxidation.

The working model of this study was curated as shown in Supp Fig S2A, which explains how PGK1 and PDH influence ferroptosis sensitivity under normoxic and hypoxic conditions. This diagram connects our findings with known metabolic pathways to provide a merged mechanistic framework. While we show that genetic and pharmacologic modulation of PGK1 alters ferroptosis sensitivity and redox balance, we acknowledge that not all observed relationships imply direct causation at the level of individual metabolic fluxes. An important mechanistic insight from this study is that PDH downregulation and GPX4 destabilization occur in parallel rather than in a hierarchical manner following PGK1 depletion. Thus, while PDH influences metabolic flexibility and ferroptosis sensitivity through mitochondrial oxidative metabolism on one hand, GPX4 independently regulates lipid peroxide detoxification and ferroptosis execution on the other. This was validated by the GPX4 overexpression experiments, which mitigated ferroptosis sensitivity without restoring PDH, suggesting cooperation between these pathways in ferroptosis sensitization.

In this study, we show the therapeutic potential of targeting PGK1 in combination with ferroptosis-inducing agents. Although we observed that IKE treatment shrinks tumors in immune-competent

BALB/c mice, the effect of PGK1 depletion during IKE treatment is striking, which shows the abrogation of both micro and macroscopic tumor metastasis to the lungs. Beyond its role in glycolysis and immunomodulation, PGK1 has been reported to regulate autophagy and survival through the stress-linked AMPK-mTOR signaling axis. Interestingly, the therapeutic combination of activators of the AMPK-mTOR pathway, such as metformin and rapamycin, has shown strong efficacy in TNBC models [34-36], leaving a window to explore co-targeting PGK1 with modulators of the AMPK-mTOR pathway for ferroptosis enhancement. Moreover, promising inhibitors such as CBR-470-1 and Ilicicolin H, which disrupt PGK1 enzymatic activity, and concurrently inhibit PGK1 and mitochondrial complex III, respectively, have been reported to exhibit anticancer effects in preclinical models [37] The success recorded by these strategies in cancer treatment indicates that PGK1 is a druggable target, which, when combined with the approaches mentioned earlier, can potentially broaden therapeutic strategies, especially in metabolically active and therapy-resistant subtypes of malignancies such as TNBC.

Taken together, this study identifies PGK1 as a mediator of ferroptosis resistance and provides a rationale for targeting PGK1 in conjunction with ferroptosis induction as a potential therapeutic strategy for aggressive breast cancers such as TNBC. By simultaneously inhibiting tumor growth and enhancing ferroptosis sensitization, this approach might offer a multifaceted attack on cancer cells for improving response to ferroptosis induction.

Declarations

Ethics approval and consent to participate

Not applicable

Consent for publication

Not applicable

Availability of Data and Materials

The datasets reported in this study are available in GEO under accession number GSE148297.

The preprint version of this work can be accessed online at: https://doi.org/10.21203/rs.3.rs-7323200/v1

Clinical Trial Number

Not applicable

Artificial intelligence usage statement

The authors used ChatGPT (OpenAI) for minor language editing and grammar improvement. The authors reviewed and verified all outputs and take full responsibility for the content of the manuscript.

Funding

This investigation was self-funded by the Yang Lab.

Author Contribution

FO performed some bioinformatic investigation into PGK1 expression across a. cancer subtypes, and b. tumor staging. She also analyzed the raw data from the PDH depletion experiments using statistical tools. TO conducted a bioinformatic analysis of the prognostic significance of PGK1 expression in relation to post-progression survival, relapse-free survival, and overall survival in patients with luminal and HER2-positive breast cancer. OO conducted a bioinformatic investigation into the differences between sensitive and ferroptosis-resistant cell lines using GEO datasets. He also investigated the Protein and gene expression of PGK1 across various tissues and their corresponding tumors. AA brought in his methods for evaluating different protein expressions of PGK1 downstream targets. He also reviewed the draft of this manuscript. XR and SN revised and sourced resources to carry out this research work. CN and AS worked on the curation of Data as well as their validation for this research work. XR and JY supervised and sourced funds and resources to carry out this research work. At the time of this work, OO, AA, CN, AS, S N, XR, X R, and JY were affiliated with the Department of Toxicology and Cancer Biology, University of Kentucky, USA. FO was affiliated with the Department of Microbiology, University of Ilorin, Nigeria. TO was an independent bioinformatics collaborator based in Manitoba, Canada.

5. References

1. Giaquinto AN, Sung H, Newman LA, Freedman RA, Smith RA, Star J, Jemal A, Siegel RL: **Breast cancer statistics 2024**. *CA Cancer J Clin* 2024, **74**(6):477–495. doi:10.3322/caac.21863:
2. Siegel RL, Giaquinto AN, Jemal A: **Cancer statistics, 2024**. *CA Cancer J Clin* 2024, **74**(1):12–49. doi:10.3322/caac.21820:
3. Faubert B, Solmonson A, DeBerardinis RJ: **Metabolic reprogramming and cancer progression**. *Science* 2020, **368**(6487). doi:10.1126/science.aaw5473: PMC7227780.

4. McCann C, Kerr EM: **Metabolic Reprogramming: A Friend or Foe to Cancer Therapy?** *Cancers (Basel)* 2021, **13**(13). doi:10.3390/cancers13133351: PMC8267696.
5. Schiliro C, Firestein BL: **Mechanisms of Metabolic Reprogramming in Cancer Cells Supporting Enhanced Growth and Proliferation**. *Cells* 2021, **10**(5). doi:10.3390/cells10051056: PMC8146072.
6. Lei G, Zhuang L, Gan B: **Targeting ferroptosis as a vulnerability in cancer**. *Nat Rev Cancer* 2022, **22**(7):381–396. doi:10.1038/s41568-022-00459-0: PMC10243716.
7. Chen Z, Wang W, Abdul Razak SR, Han T, Ahmad NH, Li X: **Ferroptosis as a potential target for cancer therapy**. *Cell Death Dis* 2023, **14**(7):460. doi:10.1038/s41419-023-05930-w: PMC10366218.
8. Zhang C, Liu X, Jin S, Chen Y, Guo R: **Ferroptosis in cancer therapy: a novel approach to reversing drug resistance**. *Mol Cancer* 2022, **21**(1):47. doi:10.1186/s12943-022-01530-y: PMC8840702.
9. Fu Q, Yu Z: **Phosphoglycerate kinase 1 (PGK1) in cancer: A promising target for diagnosis and therapy**. *Life Sci* 2020, **256**:117863. doi:10.1016/j.lfs.2020.117863:
10. Liu H, Wang X, Shen P, Ni Y, Han X: **The basic functions of phosphoglycerate kinase 1 and its roles in cancer and other diseases**. *Eur J Pharmacol* 2022, **920**:174835. doi:10.1016/j.ejphar.2022.174835:
11. Zhang K, Sun L, Kang Y: **Regulation of phosphoglycerate kinase 1 and its critical role in cancer**. *Cell Commun Signal* 2023, **21**(1):240. doi:10.1186/s12964-023-01256-4: PMC10506215.
12. Liu J, Lichtenberg T, Hoadley KA, Poisson LM, Lazar AJ, Cherniack AD, Kovatich AJ, Benz CC, Levine DA, Lee AV *et al*: **An Integrated TCGA Pan-Cancer Clinical Data Resource to Drive High-Quality Survival Outcome Analytics**. *Cell* 2018, **173**(2):400–416 e411. doi:10.1016/j.cell.2018.02.052: PMC6066282.
13. Ghoochani A, Hsu EC, Aslan M, Rice MA, Nguyen HM, Brooks JD, Corey E, Paulmurugan R, Stoyanova T: **Ferroptosis Inducers Are a Novel Therapeutic Approach for Advanced Prostate Cancer**. *Cancer Res* 2021, **81**(6):1583–1594. doi:10.1158/0008-5472.CAN-20-3477: PMC7969452.
14. Yang F, Xiao Y, Ding JH, Jin X, Ma D, Li DQ, Shi JX, Huang W, Wang YP, Jiang YZ *et al*: **Ferroptosis heterogeneity in triple-negative breast cancer reveals an innovative immunotherapy combination strategy**. *Cell Metab* 2023, **35**(1):84–100 e108. doi:10.1016/j.cmet.2022.09.021:
15. Gao X, Pan T, Gao Y, Zhu W, Liu L, Duan W, Han C, Feng B, Yan W, Song Q *et al*: **Acetylation of PGK1 at lysine 323 promotes glycolysis, cell proliferation, and metastasis in luminal A breast cancer cells**. *BMC Cancer* 2024, **24**(1):1054. doi:10.1186/s12885-024-12792-8: PMC11348675.
16. Guo Z, Zhang Y, Wang H, Liao L, Ma L, Zhao Y, Yang R, Li X, Niu J, Chu Q *et al*: **Hypoxia-induced downregulation of PGK1 crotonylation promotes tumorigenesis by coordinating glycolysis and the TCA cycle**. *Nat Commun* 2024, **15**(1):6915. doi:10.1038/s41467-024-51232-w: PMC11319824.
17. Holliday DL, Speirs V: **Choosing the right cell line for breast cancer research**. *Breast Cancer Res* 2011, **13**(4):215. doi:10.1186/bcr2889: PMC3236329.
18. Lehmann BD, Bauer JA, Chen X, Sanders ME, Chakravarthy AB, Shyr Y, Pietenpol JA: **Identification of human triple-negative breast cancer subtypes and preclinical models for selection of targeted therapies**. *J Clin Invest* 2011, **121**(7):2750–2767. doi:10.1172/JCI45014: PMC3127435.
19. Dixon SJ, Lemberg KM, Lamprecht MR, Skouta R, Zaitsev EM, Gleason CE, Patel DN, Bauer AJ, Cantley AM, Yang WS *et al*: **Ferroptosis: an iron-dependent form of nonapoptotic cell death**. *Cell* 2012, **149**(5):1060–1072. doi:10.1016/j.cell.2012.03.042: PMC3367386.
20. Hangauer MJ, Viswanathan VS, Ryan MJ, Bole D, Eaton JK, Matov A, Galeas J, Dhruv HD, Berens ME, Schreiber SL *et al*: **Drug-tolerant persister cancer cells are vulnerable to GPX4 inhibition**. *Nature* 2017, **551**(7679):247–250. doi:10.1038/nature24297: PMC5933935.
21. Li X, Jiang Y, Meisenhelder J, Yang W, Hawke DH, Zheng Y, Xia Y, Aldape K, He J, Hunter T *et al*: **Mitochondria-Translocated PGK1 Functions as a Protein Kinase to Coordinate Glycolysis and the TCA Cycle in Tumorigenesis**. *Mol Cell* 2016, **61**(5):705–719. doi:10.1016/j.molcel.2016.02.009: PMC4888784.
22. Zhang Y, Yu G, Chu H, Wang X, Xiong L, Cai G, Liu R, Gao H, Tao B, Li W *et al*: **Macrophage-Associated PGK1 Phosphorylation Promotes**

Aerobic Glycolysis and Tumorigenesis. *Mol Cell* 2018, **71**(2):201–215 e207. doi:10.1016/j.molcel.2018.06.023:

23. Tang SJ, Ho MY, Cho HC, Lin YC, Sun GH, Chi KH, Wang YS, Jhou RS, Yang W, Sun KH: **Phosphoglycerate kinase 1-overexpressing lung cancer cells reduce cyclooxygenase 2 expression and promote anti-tumor immunity in vivo**. *Int J Cancer* 2008, **123**(12):2840–2848. doi:10.1002/ijc.23888:
24. Zheng J, Conrad M: **The Metabolic Underpinnings of Ferroptosis**. *Cell Metab* 2020, **32**(6):920–937. doi:10.1016/j.cmet.2020.10.011:
25. Kim JW, Lee JY, Oh M, Lee EW: **An integrated view of lipid metabolism in ferroptosis revisited via lipidomic analysis**. *Exp Mol Med* 2023, **55**(8):1620–1631. doi:10.1038/s12276-023-01077-y: PMC10474074.
26. Zhang Y, Xin L, Xiang M, Shang C, Wang Y, Wang Y, Cui X, Lu Y: **The molecular mechanisms of ferroptosis and its role in cardiovascular disease**. *Biomed Pharmacother* 2022, **145**:112423. doi:10.1016/j.biopha.2021.112423:
27. Leu JI, Murphy ME, George DL: **Functional interplay among thiol-based redox signaling, metabolism, and ferroptosis unveiled by a genetic variant of TP53**. *Proc Natl Acad Sci U S A* 2020, **117**(43):26804–26811. doi:10.1073/pnas.2009943117: PMC7604449.
28. Vuckovic AM, Venerando R, Tibaldi E, Bosello Travain V, Roveri A, Bordin L, Miotto G, Cozza G, Toppo S, Maiorino M *et al*: **Aerobic pyruvate metabolism sensitizes cells to ferroptosis primed by GSH depletion**. *Free Radic Biol Med* 2021, **167**:45–53. doi:10.1016/j.freeradbiomed.2021.02.045:
29. Liu H, Wang S, Wang J, Guo X, Song Y, Fu K, Gao Z, Liu D, He W, Yang LL: **Energy metabolism in health and diseases**. *Signal Transduct Target Ther* 2025, **10**(1):69. doi:10.1038/s41392-025-02141-x: PMC11836267.
30. Kumar V, Greenberg ML: **Emerging roles of pyruvate dehydrogenase phosphatase 1: a key player in metabolic health**. *Front Physiol* 2025, **16**:1596636. doi:10.3389/fphys.2025.1596636: PMC12146199.
31. Guo B, Zhang F, Yin Y, Ning X, Zhang Z, Meng Q, Yang Z, Jiang W, Liu M, Wang Y *et al*: **Post-translational modifications of pyruvate dehydrogenase complex in cardiovascular disease**. *iScience* 2024, **27**(9):110633. doi:10.1016/j.isci.2024.110633: PMC11367490.
32. Fisher-Wellman KH, Lin CT, Ryan TE, Reese LR, Gilliam LA, Cathey BL, Lark DS, Smith CD, Muoio DM, Neufer PD: **Pyruvate dehydrogenase complex and nicotinamide nucleotide transhydrogenase constitute an energy-consuming redox circuit**. *Biochem J* 2015, **467**(2):271–280. doi:10.1042/BJ20141447: PMC4442697.
33. Kim JW, Tchernyshyov I, Semenza GL, Dang CV: **HIF-1-mediated expression of pyruvate dehydrogenase kinase: a metabolic switch required for cellular adaptation to hypoxia**. *Cell Metab* 2006, **3**(3):177–185. doi:10.1016/j.cmet.2006.02.002:
34. Qiu A, Wen X, Zou Q, Yin L, Zhu S, Sheng Y, He Y, Liu Q, Luo D, Guo Z: **Phosphoglycerate Kinase 1: An Effective Therapeutic Target in Cancer**. *Front Biosci (Landmark Ed)* 2024, **29**(3):92. doi:10.31083/j.fbl2903092:
35. Mukhopadhyay S, Chatterjee A, Kogan D, Patel D, Foster DA: **5-Aminoimidazole-4-carboxamide-1-beta-4-ribofuranoside (AICAR) enhances the efficacy of rapamycin in human cancer cells**. *Cell Cycle* 2015, **14**(20):3331–3339. doi:10.1080/15384101.2015.1087623: PMC4825547.
36. Qian X, Li X, Cai Q, Zhang C, Yu Q, Jiang Y, Lee JH, Hawke D, Wang Y, Xia Y *et al*: **Phosphoglycerate Kinase 1 Phosphorylates Beclin1 to Induce Autophagy**. *Mol Cell* 2017, **65**(5):917–931 e916. doi:10.1016/j.molcel.2017.01.027: PMC5389741.
37. Zheng J, Zhu JL, Zhang Y, Zhang H, Yang Y, Tang DR, Sun J: **PGK1 inhibitor CBR-470-1 protects neuronal cells from MPP+**. *Aging (Albany NY)* 2020, **12**(13):13388–13399. doi:10.18632/aging.103443: PMC7377839.

List of abbreviations

Abbreviation	Full Form
2-DG	2-Deoxy-D-glucose
ACSL4	Acyl-CoA synthetase long-chain family member 4
AMPK	AMP-activated protein kinase
ANOVA	Analysis of Variance
ATP	Adenosine triphosphate
BCA	Bicinchoninic Acid
CD25	Cluster of Differentiation 25
CD71	Cluster of Differentiation 71
DAPI	4â€²,6-diamidino-2-phenylindole
DMEM	Dulbeccoâ€™s Modified Eagle Medium
DMSO	Dimethyl Sulfoxide
ECAR	Extracellular Acidification Rate
FBS	Fetal Bovine Serum
FFPE	Formalin-Fixed Paraffin-Embedded
GEO	Gene Expression Omnibus
GPX4	Glutathione Peroxidase 4
HRP	Horseradish Peroxidase
IC50	Half maximal inhibitory concentration
IKE	Imidazole Ketone Erastin
KM	Kaplan-Meier
LDHA	Lactate Dehydrogenase A
OS	Overall Survival
PBS	Phosphate Buffered Saline
PBST	PBS with Tween 20
PDH	Pyruvate Dehydrogenase
PGK1	Phosphoglycerate Kinase 1
PPS	Post-Progression Survival
PVDF	Polyvinylidene Fluoride
RFS	Relapse-Free Survival
RNA	Ribonucleic Acid
RPMI	Roswell Park Memorial Institute medium
SD	Standard Deviation
SDS-PAGE	Sodium Dodecyl Sulfateâ“Polyacrylamide Gel Electrophoresis
TCA	Tricarboxylic Acid
TCGA	The Cancer Genome Atlas
TME	Tumor Microenvironment
TNBC	Triple-Negative Breast Cancer
cDNA	Complementary DNA
Mtor	Mechanistic Target of Rapamycin
qRT-PCR	Quantitative Real-Time Polymerase Chain Reaction
ShRNA	Short Hairpin RNA
SiRNA	Small Interfering RNA
4-HNE	4-hydroxynonenal

Supplementary Fig. S1. PGK1 Depletion and Ferroptosis Sensitivity in Breast Cancer Cells. A. Representative images of PGK1 and GPX4 staining in control and PGK1-depleted MCF7 cell line and their quantification. **B.** Representative images and quantification of crystal violet-stained colonies in MCF7 cells and **C.** 4T1 cells treated with vehicle, erastin (1.25 μM), NG52 (5 μM), or their combination. **D.** Representative images of control and stable PGK1-depleted 4T1 and MDAMB231 cell lines. **E.** Percentage Cell viability analysis of human MDAMB231 and **F.** murine 4T1 carcinomas after treatment with vehicle, erastin only, or in combination with cell death inhibitors ZVAD-FMK, Liproxstatin, Ferrostatin, and N-acetyl-cysteine (NAC). Mean ± SD; one-way ANOVA, ns: not significant, * $p < 0.05$, ** $p < 0.01$, *** $p < 0.001$, **** $p < 0.0001$.

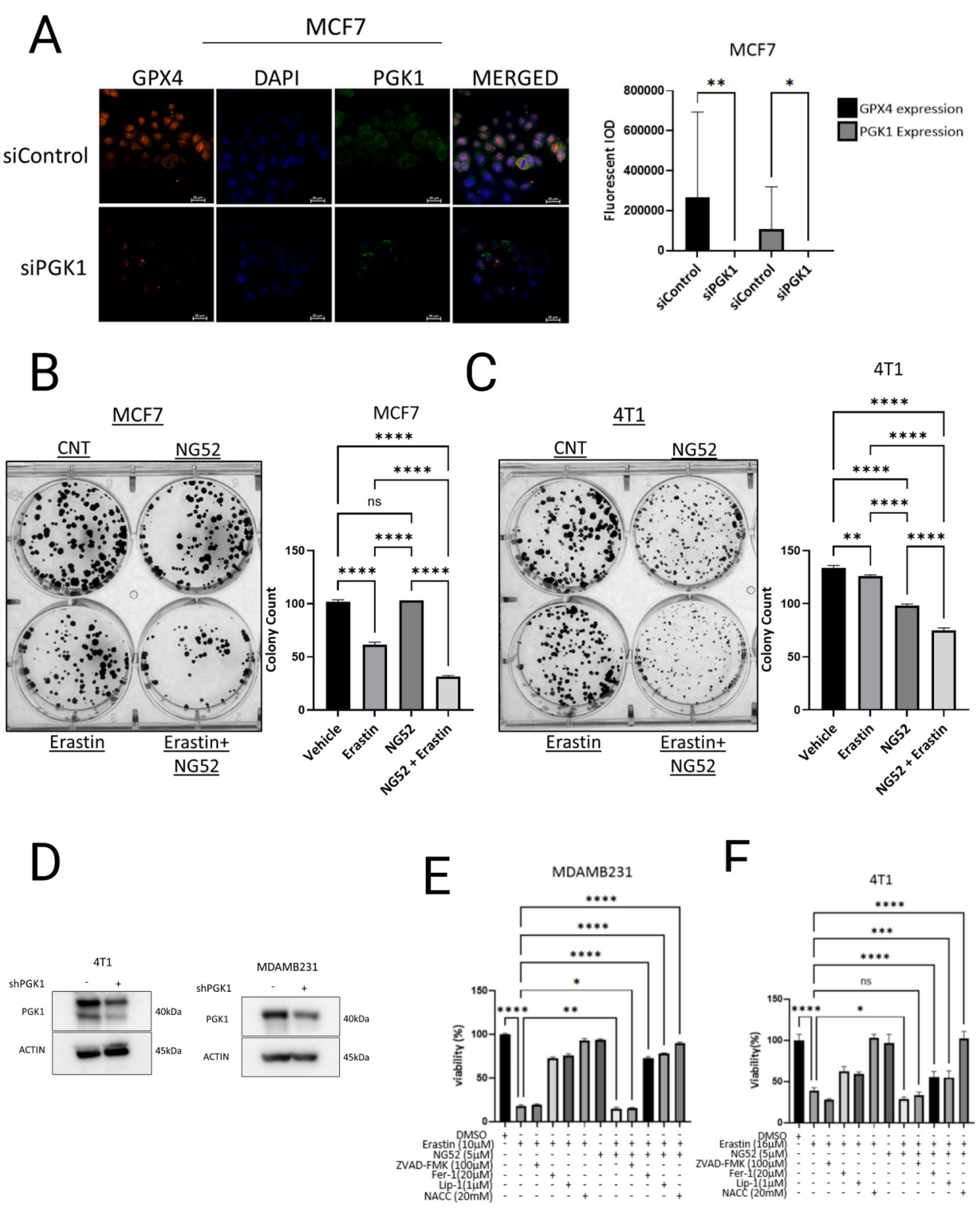

Supplementary Fig. S2. PGK1 regulates ferroptosis sensitivity and patient prognosis in breast cancer. A schematic model illustrates how PGK1 maintains PDH-dependent mitochondrial metabolism and cooperates in parallel with GPX4 to preserve redox homeostasis, thereby restraining ferroptosis. **B.** Percentage Cell viability analysis of MDAMB231 cells after treatment with vehicle, erastin, siRNA (PGK1), or their combination. **C.** Kaplan-Meier survival curves showing that high PGK1 expression correlates with shorter post-progression survival. **D.** High PGK1 expression correlates with shorter Relapse-Free Survival in BC. **E** High PGK1 expression correlates with shorter Overall Survival (OS) in Luminal A BC but not in **F.** HER2-enriched breast cancer (p = 0.36). or **G.** Triple-Negative breast cancer (p = 0.2). Data source: Kaplan-Meier Plotter (Győrffy et al., Comput. Struct. Biotechnol. J. 2021), integrating GEO Affymetrix microarray and TCGA RNA-seq cohorts with OS, RFS, and DFS endpoints. Mean ± SD; one-way ANOVA, ns: not significant, * $p < 0.05$, ** $p < 0.01$, *** $p < 0.001$, **** $p < 0.0001$.

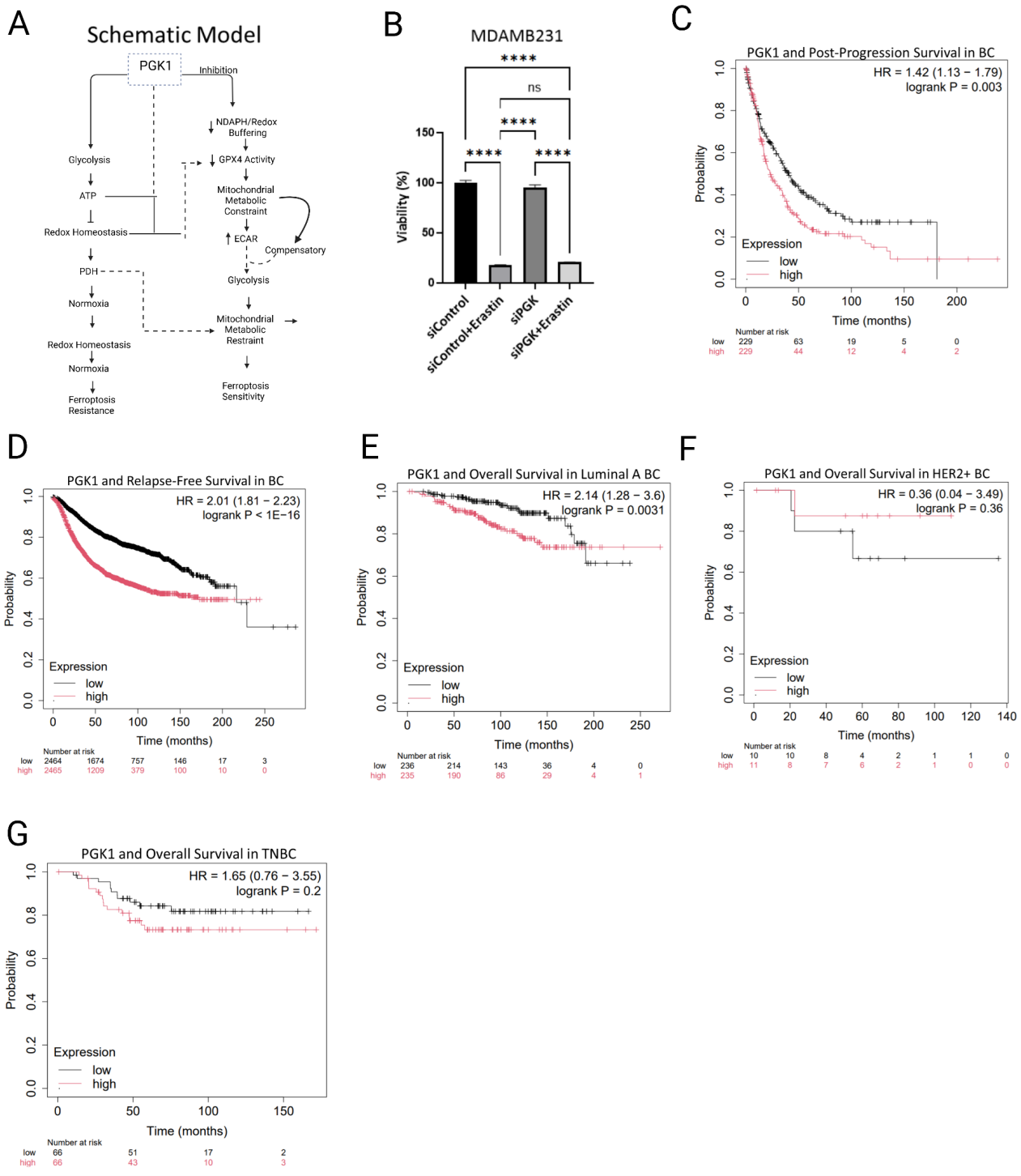

Supplementary Fig. S3. Validation of PGK1-dependent ferroptosis sensitization using an independent PGK1 inhibitor. **A.** Percentage cell viability of MDAMB231, 4T1, and MDAMB468 cells after treatment with vehicle, the alternative PGK1 inhibitor Z57346765, erastin, or their combination with or without Fer-1 for 72 hours. **B.** Western blotting Image of PGK1, ferroptosis, and metabolism-associated proteins in MDAMB231 and MCF7 cells treated with vehicle, erastin, Z57346765, or their combination. Statistical significance was determined by one-way ANOVA (panel A) with appropriate multiple-comparison testing. **C.** Immunofluorescence staining of GPX4 expression in MDAMB468 cells that were treated with vehicle, erastin, NG52, or their combinations, with or without ferroptosis ferrostatin-1 or liproxstatin-1. * $p < 0.05$, ** $p < 0.01$, *** $p < 0.001$, **** $p < 0.0001$; ns, not significant. Data are presented as mean ± SD from n = 3 independent experiments.

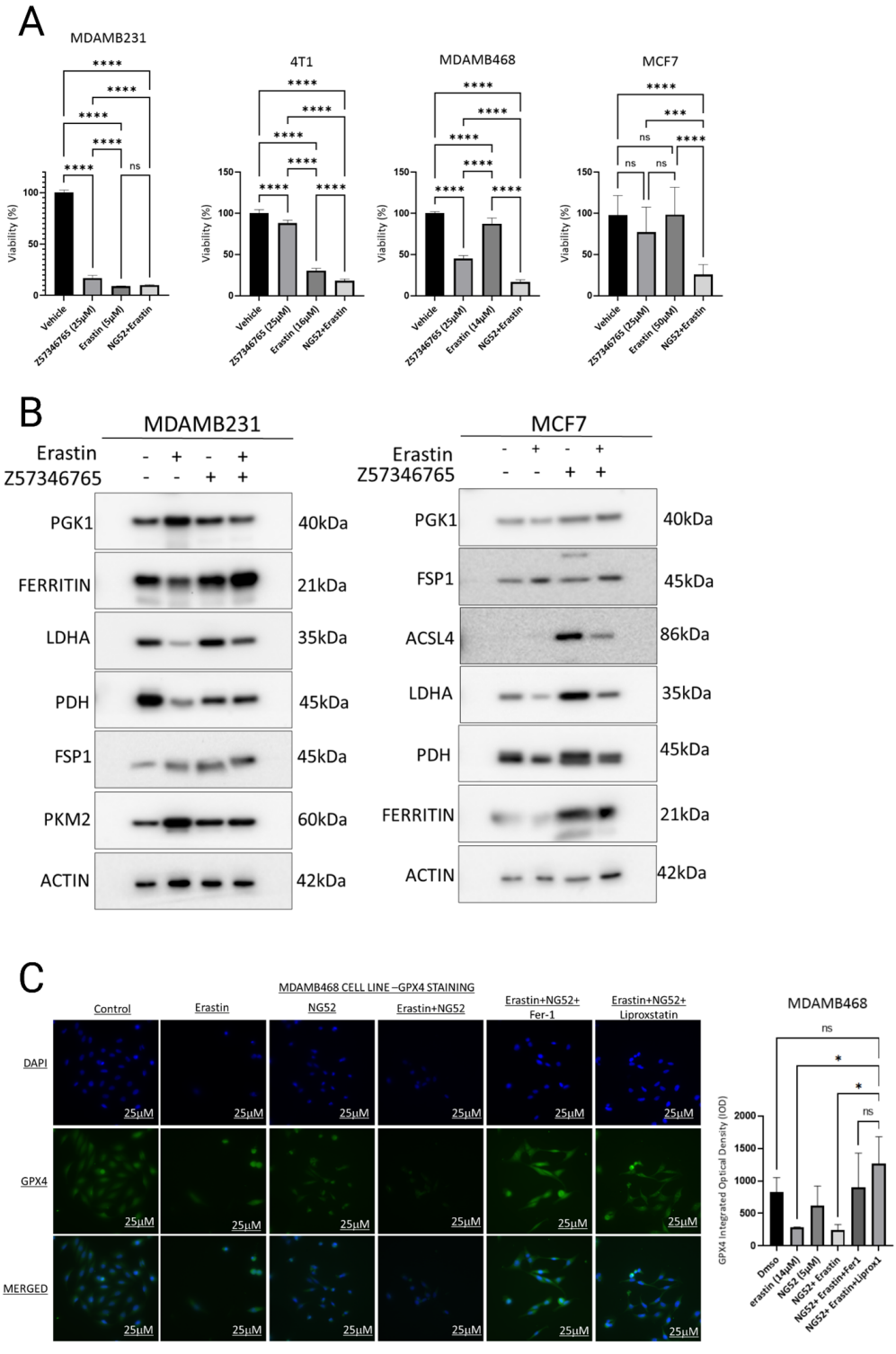

Supplementary Fig. S4. PGK1 depletion promotes ferroptosis-associated lipid peroxidation
A. Representative images of 4-hydroxynonenal (4-HNE) immunohistochemical staining of 4T1 tumor sections from shC and shPGK1 tumors treated with vehicle or IKE, and their quantification. **B.** Representative flow cytometry dot plots of C11-BODIPY 581/591 staining in**.** 4T1, **C.** MDAMB231, and **D.** MCF7 cells treated with vehicle, erastin, NG52, or their combination, in the presence or absence of ferrostatin-1 or liproxstatin-1. Data are presented as mean ± SD from n = 3 independent experiments. Statistical significance was determined by one-way ANOVA (panel A) with appropriate multiple-comparison testing. * $p < 0.05$, ** $p < 0.01$, *** $p < 0.001$, **** $p < 0.0001$; ns, not significant.